Journal of The Electrochemical Society

OPEN ACCESS

Development of a New Procedure for Nail Penetration of Lithium-Ion Cells to Obtain Meaningful and Reproducible Results

Journal of The Electrochemical Society, 2020 **167** 090504

Development of a New Procedure for Nail Penetration of Lithium-Ion Cells to Obtain Meaningful and Reproducible Results

Jan Diekmann,[z] Stefan Doose, Svenja Weber, Swantje Münch, Wolfgang Haselrieder, and Arno Kwade

Institute of Particle Technology, TU Braunschweig, Lower Saxony, Germany

Internal short circuit tests of Lithium-Ion Batteries (LIBs) are used to test battery safety behavior in a custom made battery cell stressing chamber. However, systematic investigations regarding the test setup and test procedure are rare. In our research commercially available pouch cells (5 Ah) are employed for the method development and validation of nail penetration tests including measurement of gaseous reaction products. The effects of the thermal insulation material, the nail material (conductive and non-conductive), the influence of the penetration depth and the nail velocity were examined. It was observed that low penetration velocities (1 mm s^{-1}) in combination with a conductive nail and a nail motion control, which is based on monitoring the temporal evaluation of the cell voltage change, provide the most promising results in terms of reproducibility at low standard deviation. By applying this method, only the energy required for a Thermal Runaway (TR) is released, which makes it possible to determine a novel key value for the assessment of battery safety. Based on this, a proposal has been made for a nail penetration test method which would allow the results to be compared between different test facilities.
 [DOI: 10.1149/1945-7111/ab78ff]

Manuscript submitted November 22, 2019; revised manuscript received January 29, 2020. Published March 12, 2020. *This paper is part of the JES Focus Issue on Battery Safety, Reliability and Mitigation.*

Supplementary material for this article is available online

Increasing usage of Lithium-Ion Batteries (LIBs) in portable devices and electric vehicles (EVs) is mainly based on their high specific energy, high energy density and long cycle life.[1–3] In light of this development it is essential that new high energy batteries are safe within operation conditions as well as in critical situations.[4,5] For this reason, safety studies on LIBs, particularly in regards to the risks of thermal runaway (TR), are getting more attention than ever before. Most of today's testing methods, e.g. nail penetration, crush, mechanical shock, overcharge, are described in literature and standards (UN T 38.3, UN ECE R 100, ISO 12405 1-3, SAE J 2464, SAE J 2929, QC/T 743). However, there is hardly no standardization and systematic investigation work published so far.[6–8] Especially the comparison between test results of different test facilities is only possible with very high investigative effort. Because of these circumstances there is a great necessity for a standardized and validated test methodology in battery abuse testing. Otherwise conclusions could be variable and have low informative value.

Among the various abuse testing regulations of LIBs the internal short circuit represents one of the most critical cases. In field operation internal short circuits can be triggered by different mechanisms like mechanical damage[9,10] or production failure (Samsung Note 7). Generally, for scientific work nail penetration testing is widely used to investigate the effects of the internal short circuit in LIBs. Nail penetration causes an internal electrode or separator failure where a current path evolves within the battery, which, according to Joule's First law, leads to heat generation due to internal resistance. Depending on the amount of heat produced during the short circuit, the cell goes into TR or stays in safe conditions during the forced discharge process. Exothermal chemical reactions within a TR start with the decomposition of the solid electrolyte interface (SEI) at 90 °C−120 °C followed by the reaction of intercalated lithium with the electrolyte at >120 °C. Thereafter the decomposition of the electrolyte (> 200 °C) and the reaction of intercalated lithium with binder (≈ 240 °C) takes place. The positive active material starts to decompose at > 250 °C.[11–14] From these reactions different hazardous gaseous reaction products (e.g. CO, HF) are released and a critical amount of heat generated, which can cause thermal propagation within battery modules in field operation.[15,16]

However, the short circuit mechanism is also strongly influenced by the nail material. On the one hand, conductive nail material (e.g. steel) induces a short circuit due to the nail material itself. The current flows indirectly over the nail surface into the short circuited electrode area as well as over direct electrode contact. On the other hand, using non-conductive nail material (e.g. ceramic) simply leads to a direct short circuit between the adjacent electrodes on the basis of positive and negative electrode contact.[17] Regardless, the result of heat generation is the same in both cases.

For achieving the desired target of a standardized and validated test method, a significant amount of battery abuse tests is required. In test series of a number of batteries it is essential to achieve low standard deviations of measured values during the TR.

The goal of this paper is to introduce an experimentally validated and standardized nail penetration method with very low standard deviations for single cell tests. Different external parameters and their influence on the results of battery cell nail penetration are investigated and discussed. In particular, this study shows the significant influence of different nail velocities, thermal isolation materials and nail materials (steel and ceramic) on the resulting voltage drop, formed infrared active gaseous components and temperature courses on the battery surface as well as within the nail.

Experimental

The investigations presented are performed utilizing a newly developed battery investigation chamber with its integrated actuator and sensor technology. The basic experimental setup and the materials used are described below. All results were determined by a triple determination (three repetitions of tests with identical test parameters) and thus, correspond to averaged values with standard deviations. An overview of the tests performed, the corresponding parameters and maximum measured key values can be found in the supplemental material (available online at stacks.iop.org/JES/167/090504/mmedia).

Battery cell investigation chamber.—In order to realize a measurement of the gaseous components generated during a TR,

*Electrochemical Society Member.
[z]E-mail: mail@jandiekmann.de

the battery cell investigation chamber is a gas-tight chamber with an interior volume of 15.4 l. Structure and gas flow are shown in Fig. 1a. The chamber is made of stainless steel and designed to withstand an internal pressure of 5 bar. To enable online gas analysis, gas is continuously withdrawn from the chamber and the same quantity is added. Since a large amount of gas is released in a short time during a TR, the gas is sampled by the gas analysis device via a bypass. For safety and environmental reasons, the gas exhausted from the chamber and the measuring gas from the gas analysis are fed to a gas scrubber. By this operation procedure the ambient pressure always prevails inside the chamber, but any atmosphere can be adjusted via the gas supply. The results presented here are generated under nitrogen atmosphere and alternatively with air (air from a compressed air cylinder provided at ambient pressure). In addition, the chamber is equipped with pressure and temperature measurement for the inner space. Video surveillance from outside is possible via a borosilicate inspection window.

The cell voltage is measured via crocodile clips on the terminals of the cell (compare Fig. 1c). To record the relevant cell surface temperature, two thermocouples (Type K, −100–1,100 °C) at a distance of 10 mm from the penetration point between the insulation material and the cell are attached with adhesive strips to the cell surface. The data of both thermocouples are used to determine the mean value and standard deviation of the relevant cell surface temperature.

An important component of the battery cell investigation chamber is the cell holder, as it enables the cell to be fixed in a defined state (Fig. 1b). The cell tension is exerted via tension plates

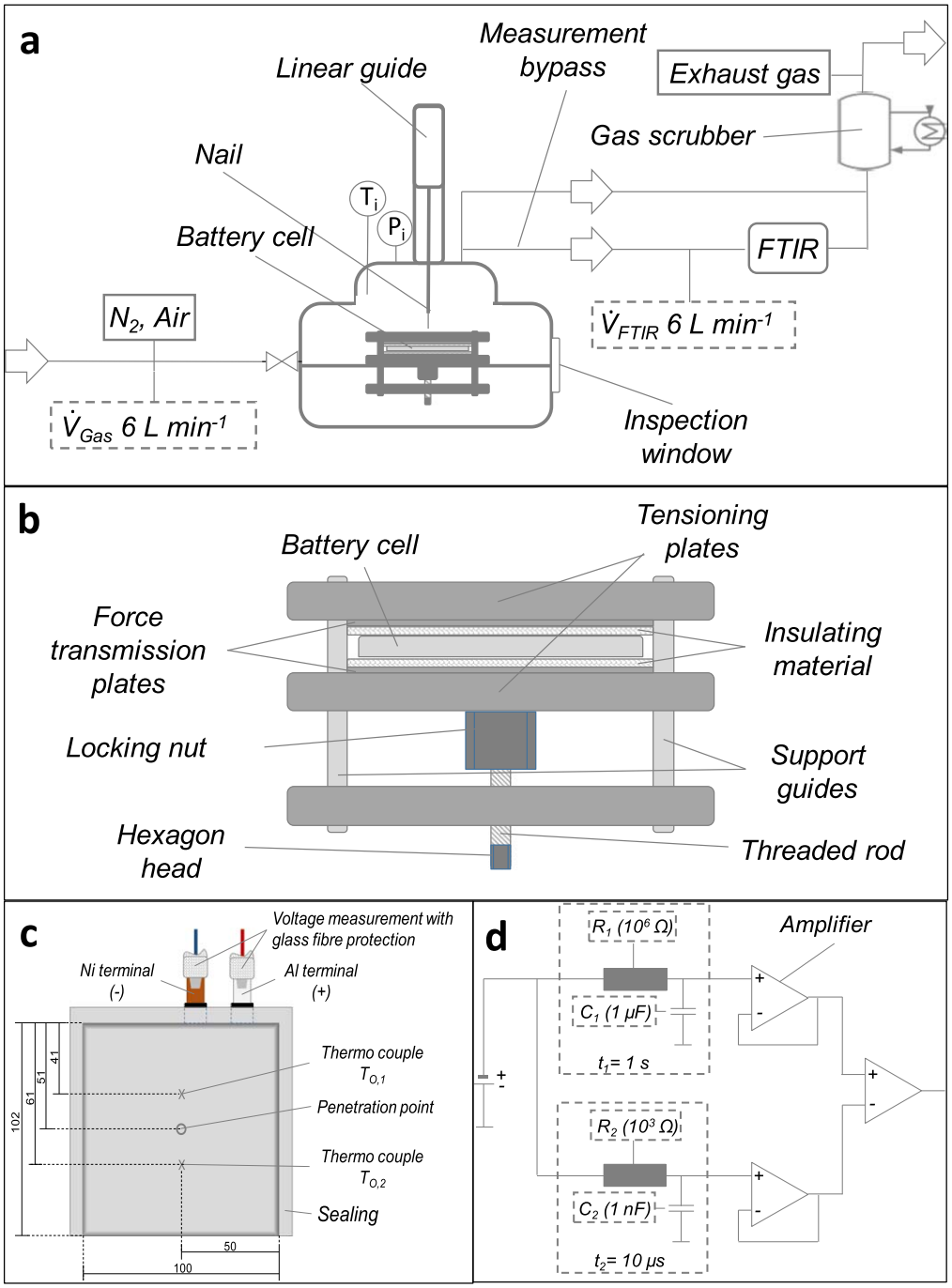

Figure 1. Illustrations of the experimental setup: Overview of the structure and gas flow of the investigation chamber (a), scheme of the battery cell holder (b), positioning of sensors at the battery cell (c), and extract of the circuit logic of the voltage-based nail control (d).

with the surface area of the electrodes of the battery cell. The lower plate is guided over rods, while the upper plate is fixed. The force is adjusted via the torque. For this study a compression of 0.48 MPa is used.

Nail and nail control variations.—Two nail variants were used. One is made of a stainless steel with a longitudinal hole for a thermocouple inside. Therefore, a measurement of the actual nail temperature according to Hatcher et al.[17] is realized. The non-conductive nail is made of zirconium oxide. Both nails have a diameter of 3 mm. While the tip angle of the conductive nail is 30°, it is limited to 45° in the non-conductive version for manufacturing reasons. Since the short-circuit mechanism is different for both nails (see section 3), this circumstance has no influence on the outcome.

The nail guidance and control is realized by an electric linear actuator. The minimum step of the linear guide which can be controlled in a predefined way is limited to 0.5 mm. The targeted nail penetration point is the centre of the cell. The tests to determine the influence of the atmosphere are carried out with a nail speed v_N of 80 mm s^{-1}.

Measurement and approach of the penetration depth s_P through the cell (1 cell thickness) and into the middle of the cell (0.5 cell thickness) is executed by distance control. In order to determine the minimum penetration depth, the nail is manually moved on step by step until the TR occurs. These tests are all carried out with a nail speed of 80 mm s^{-1}.

In order to further increase the path resolution and to obtain a statement about the necessary penetration depth for triggering the TR, the voltage-based nail control was developed. An extract of the established electronic circuit is shown in Fig. 1d. It is based on the evaluation of the time of a cell voltage change, in which the battery cell voltage U_{cell} is compared with each other via two resistance capacitor elements (RC elements). The time constants of the two RC elements are calculated as follows:

$$t_1 = R_1 \cdot C_1 = 10^6 \Omega \cdot 10^{-6}\, F = 1\, s \quad [1]$$

$$t_2 = R_2 \cdot C_2 = 10^3\, \Omega \cdot 10^{-9} F = 10\, \mu s \quad [2]$$

$t_{1,2}$: time constants of the RC elements [s]
$R_{1,2}$: electrical resistance [Ω]
$C_{1,2}$: electrical capacitor capacity [F]

A sufficient change in cell voltage leads to a current that stops the nail advance. The nail is moved step by step quickly after the first stop until the TR was triggered (depending on test parameters approx. 0.1 V s^{-1} at the transition of 4.0 V).

The following parameters are used to describe the penetration depth s_P:

$$s_P = s_{P1} + s_{rel,P} \quad [3]$$

s_P: absolute penetration depth [mm]
s_{P1}: penetration depth until the first voltage change is detected [mm]
$s_{rel,P}$: relevant penetration depth [mm]

The relevant penetration depth $s_{rel,P}$ is defined as the path between first detected voltage change and TR.

Gas analysis.—For the gas analysis a Fourier-transform Infrared Spectroscopy (FTIR) is used in combination with a gas sampling system diluting the gas from the chamber. The sampling system contains a particle filter (filter pore size: 3 μm) and enables continuous sampling with a constant volume flow of 6 l min^{-1} (Fig. 1a). Furthermore, a thermostatized gas transport from the battery cell investigation chamber to the outlet from the measuring chamber at 180 °C is set via the sampling system and heated hoses.

The FTIR measuring chamber has an optical path length of 500 cm by multiple reflection and a spectral resolution of 7.7 cm^{-1} in the Mercury-cadmium-telluride (MCT)-detector. The quantitative evaluation of infrared active gas components is performed by simultaneous comparison with reference spectra of the corresponding components in defined wavenumber ranges. The gas components water (H_2O), carbon dioxide (CO_2), carbon monoxide (CO), hydrogen fluoride (HF), methane (CH_4), ethane (C_2H_6), ethane (C_2H_4), ethyl methyl carbonate (EMC), and ethylene carbonate (EC) are detected and determined quantitatively.

Table I. Technical data of the investigated battery cells (Kokam SLPB50106100). EMC: ethyl methyl carbonate, DMC: dimethyl carbonate, EC: ethylene carbonate, LNCO: lithium nickel cobalt oxide, LCO: lithium nickel cobalt oxide. *Manufacturer specification.

Parameter	Value
typ. capacity [Ah]*	5.5
min. capacity [Ah]*	5.0
nominal voltage [V]*	3.7
charge cut-off voltage [V]*	4.2
discharge cut-off voltage [V]*	2.7
max. discharge current [A]*	10
suspected electrolyte	EMC, EC, $LiPF_6$
cathode active material*	$LiNiCoO_2$/$LiCoO_2$
anode active material*	Graphite
weight [g]*	120
cell thickness	5.9 mm

X-ray imaging.—X-ray images of the cells before and after the nail penetration test using a conductive nail are taken by Viscom AG. The cells were irradiated from the penetration side with an X-ray inspection system (*X8011-II PCB flex*).

Investigated insulation materials.—Three materials were used to determine a suitable insulation material. All have good electrical insulation and low thermal conductivity (0.038 – 0.471 W K^{-1} m^{-1}). In addition to a non-combustible, inorganic glass fibre tape with a layer thickness of 5 mm, a phenol formaldehyde resin (Bakelite) with a layer thickness of 3 mm and a mica paper impregnated with silicone resin (DoTherm) with a layer thickness of 5 mm are tested. The materials were applied above and below the cell and provided with a hole for penetration.

Investigated cells.—For the development of this method commercial pouch cells (SLPB50106100, Kokam Ltd.) from the same production batch are used. After transport these cells showed voltages of 3.74 V on average. The cells were charged with 0.1 C (CCCV, cut off voltage 4.2 V) before the test were carried out. Further characteristic parameters of the cells are compiled in Table I.

Results and Discussion

In the following the main results regarding the development of the new nail penetration test method are presented. Different test setups and process parameters (such as nail type, gas conditions, and nail velocity) are studied according their influences on the cells safety behavior.

Atmosphere.—Besides the detailed investigations presented in the following subchapters additional experiments are carried out to determine the influence of oxygen containing atmosphere inside the test chamber. For this purpose, tests are carried out with a nail speed $v_N = 80$ mm s^{-1} under compressed air and nitrogen, both of high dryness (⩽ 5 ppm). The supplemental material belonging to this essay shows slow motion videos of tests in oxygen-containing atmosphere (compressed air) and near-exclusion of oxygen (nitrogen) as well as a summary of the test results. Under the influence of oxygen, a fast ignition of the atmosphere occurs immediately after

the short circuit. In nitrogen atmosphere (oxygen content $< 2\%$) there is no ignition, but the release of hot glowing material can be observed. The deflagration under oxygen atmosphere leads to a very high short-term increase in pressure ($\approx$ 1,48 bar, twice as high as the average maximum pressure in a nitrogen atmosphere) as well as to higher evolved temperatures of up to 122 °C in contrast to 47 °C under nitrogen atmosphere within the chamber. There is no difference in cell surface temperature for the two atmospheres. The data of the gas analysis shows the expected decrease of flammable components and increase of combustion products under presence of oxygen and differ significantly. Since the actual produced gas species are of interest to the study in order to investigate mechanisms, the change of the measured gas components is the main reason why all following tests are carried out under nitrogen atmosphere.

Insulation materials.—Especially the choice of the insulation material is of significant importance for reliable temperature measurements in order to minimize heat dissipation by the surrounding material. Therefore, a suitable insulation material should offer the highest possible thermal insulation. Simultaneously, the insulation material should be chemically inert to the reactive gas components. Furthermore, the gas flow must be able to escape from the cells without obstruction. For the interpretation of the test results the data achieved from tests without insulation serves as reference. Since all other test parameters were kept constant, differences in the developed temperatures and gas concentrations can be directly attributed to the influence of the insulation material. Figure 2 shows the average developed surface temperature that is decisive for the insulation effect of the materials.

It can be seen, that the use of an insulating material is crucial for temperature measurements, as the heat is dissipated trough the stainless steel plates of the battery holder during the tests without insulation. Although the high concentrations of CO indicate that a TR has taken place (compare Fig. 2b), only average maximum surface temperatures of 220 °C were measured. The highest surface temperatures ($\approx$ 500 °C) are achieved during the tests with glass fibre tape, despite this material having the lowest thickness. The average maximum temperatures with insulation using Bakelite and DoTherm are 465 °C and 445 °C respectively.

In this context, it must be mentioned that the standard deviations overlap due to the fact that the test method has not yet been optimized (no cell voltage-based nail control) and is therefore referred to as a trend.

A similar trend can also be seen in the concentrations of the gas components CO and HF (Figs. 2b and 2c). The concentrations are highest for both gases in the tests without insulation. An insulation should come as close as possible to these values, in order to exclude

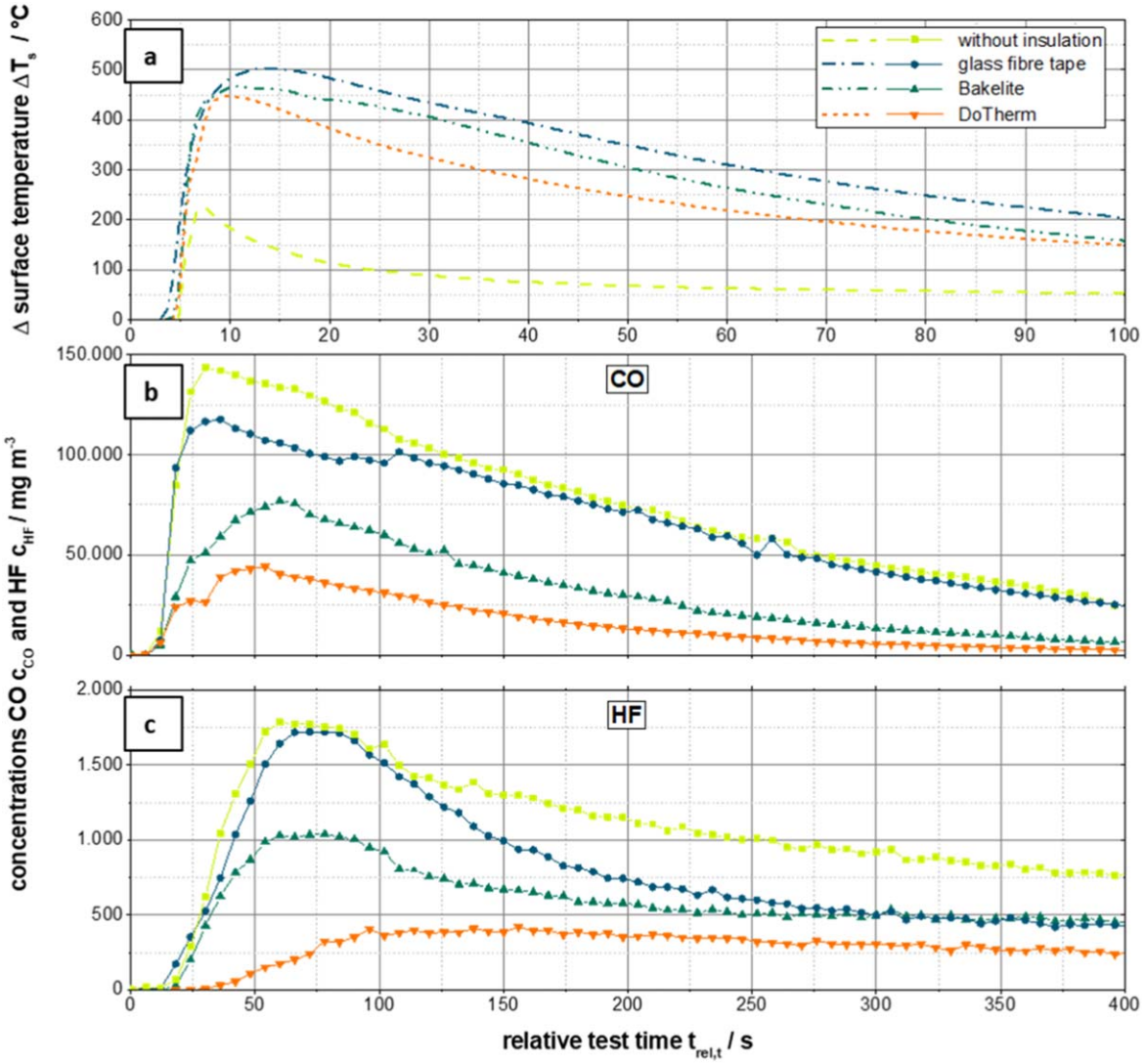

Figure 2. Average cell surface temperature ΔT_s development (a) and average concentrations of CO c_{CO} (b) and HF c_{HF} (c) as a function of relative test time $t_{rel,t}$ for different insulation materials (nail speed $v_N = 80$ mm s^{-1}). Experiments without insulation serve as reference.

a reaction of the gas components with the insulation material. Bakelite and DoTherm do not meet this requirement. Even when using glass fibre tape, the same CO concentrations are not achieved. As a possible reason a change in the outflow behavior caused by the additional layer (the insulation material) at the beginning of the cell reaction can be mentioned here. This type of blockage is not affecting the HF concentration based on the fact that HF is typically released with delay. In contrast to CO and other gas species, the maximum concentrations are reached after approximately 60 s without and even larger with insulation. Remarkable are the very low and slowly increasing gas concentrations when using DoTherm where the melting of the material with liquid release can be observed, which leads to a clogging of the gas analysis filters.

In conclusion, glass fibre tape exhibits the best thermal insulation performance of the investigated materials and the highest inertness against the guiding gas components and is therefore used for subsequent tests.

Penetration depths.—A significant influence on the cell reaction dependent on the penetration depth of the nail is suspected. The cell is short-circuited directly via the nail when a conductive material (steel nail) is used. Therefore, the cross-section of the nail within the cell stack can play a decisive role as it directly influences the short circuit current and thus, the release of Joule heat. The voltage drops for different penetration depths are depicted in Fig. 3.

The voltage drop is very similar for all penetration depths. In particular, the curves up to a relative test time of 2.5 s can be assumed to be statistically identical. In the following, this range is referred to as the initial voltage drop. Afterwards the cell voltages drop sharply due to the cell opening and melting of the separator. Finally, because of the resulting areal contact of the electrodes the cell voltage slowly decreases to 0 V. As the penetration depth increases, the time it takes for the cell voltages to reach 0 V decreases, which can be explained by the higher number of electrode layers that are short-circuited initially. However, since the initial voltage drop does not differ it can be concluded that it describes the actual short circuit, which leads to an instantaneous TR and is therefore decisive. The standard deviation increases considerably after the initial voltage drop, especially for the manually adjusted minimum penetration depth which can be explained by the limited minimum travel of the linear guide of 0.5 mm per step. Thus, the manual minimum penetration depth varies within the triple determination by this value, resulting in a higher exposed standard deviation.

The progression of surface (T_S) and nail temperatures (T_N) as well as the standard deviation of a triple determination at the maximum surface temperature $\Delta T_{S,max}$ and the maximum nail temperature $\Delta T_{N,max}$ are shown in Fig. 4.

The nail temperature varies with the penetration depth. This is due to the larger contact surface between nail and electrodes with increasing penetration depth and, therefore, higher heat transfer surface resulting in a higher maximum temperature for the penetration depth of 1.0 cell thickness. The difference between minimum penetration depth and 0.5 cell thickness is less, since the actual average penetration depths s_P differ only by 0.5 mm (2.3 mm for minimum penetration depth and 2.8 mm for 0.5 cell thickness).

The development of the cell surface temperature shows a different trend. Here, the lowest temperatures are reached at the maximum penetration depth, while the tests with lower penetration depths show higher maximum cell surface temperatures. The increased penetration depth and the larger heat transfer surface of the nail lead to a higher heat transfer to the nail and subsequently to lower surface temperatures (Fig. 4).

The differences in the measurement of the surface temperature by varying the penetration depth do not seem to have any influence on the course of the TR even if the surface temperatures differ up to about 100 °C. In general, the same can be observed for the dominant gas component CO as shown in Fig. 5. Only a minimal shift of the temporal release can be noted. This is probably due to a blocking of the gas release by the horizontal arrangement of the electrodes relative to the penetration site. The initial gas formation in a TR leads to an increase in pressure within the cell and to a reclosing of the penetration site due to the return movement of the electrodes after the initial inward bend during penetration. Since this blockage increases with a higher number of penetrated layers, there is a detectable temporal shift in the release. This effect can be observed particularly with the release of the electrolyte component EC. EC is a solid compound at room temperature with a high boiling point, and therefore, not a reaction product of the TR. The release takes place very quickly at minimum penetration depth while it decreases significantly with increasing penetration depth.

Particular attention must be paid to standard deviations when developing a method. The relative standard deviation of the maximum nail temperature $\Delta T_{N,max}$ in Fig. 4 is comparatively high and shows a decrease with increasing penetration depth of the nail. The decrease is due to the number of short-circuited electrode layers. With a higher number, i.e. a higher penetration depth, deviations in penetration depth have less influence. At the maximum penetration depth of 1 cell thickness the number of electrode layers being penetrated stays the same, but the relative standard deviation remains at a high level of 7.5%. Conclusively, the nail temperature is not considered suitable for an evaluation of a TR.

The relative standard deviations of the maximum surface temperature $T_{s,max}$ are lower. The tests with a minimum penetration depth show the smallest deviation of 1.5%, which rises to 5.7% with increasing penetration depth. As previously mentioned, the reason

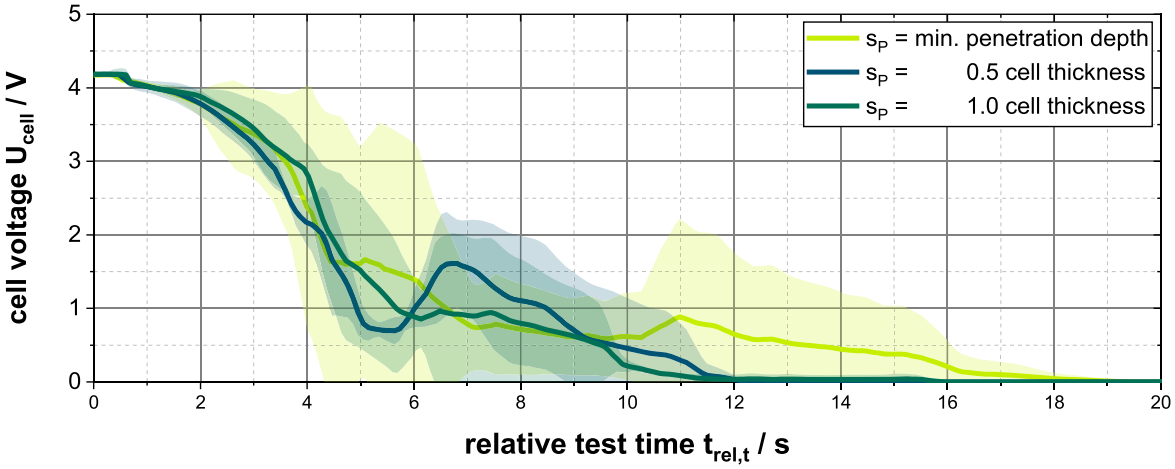

Figure 3. Average cell voltage U_{cell} as a function of the relative test time $t_{rel,t}$ for different nail penetration depths at a nail speed v_N= 80 mm s^{-1} (standard deviation of a triple determination).

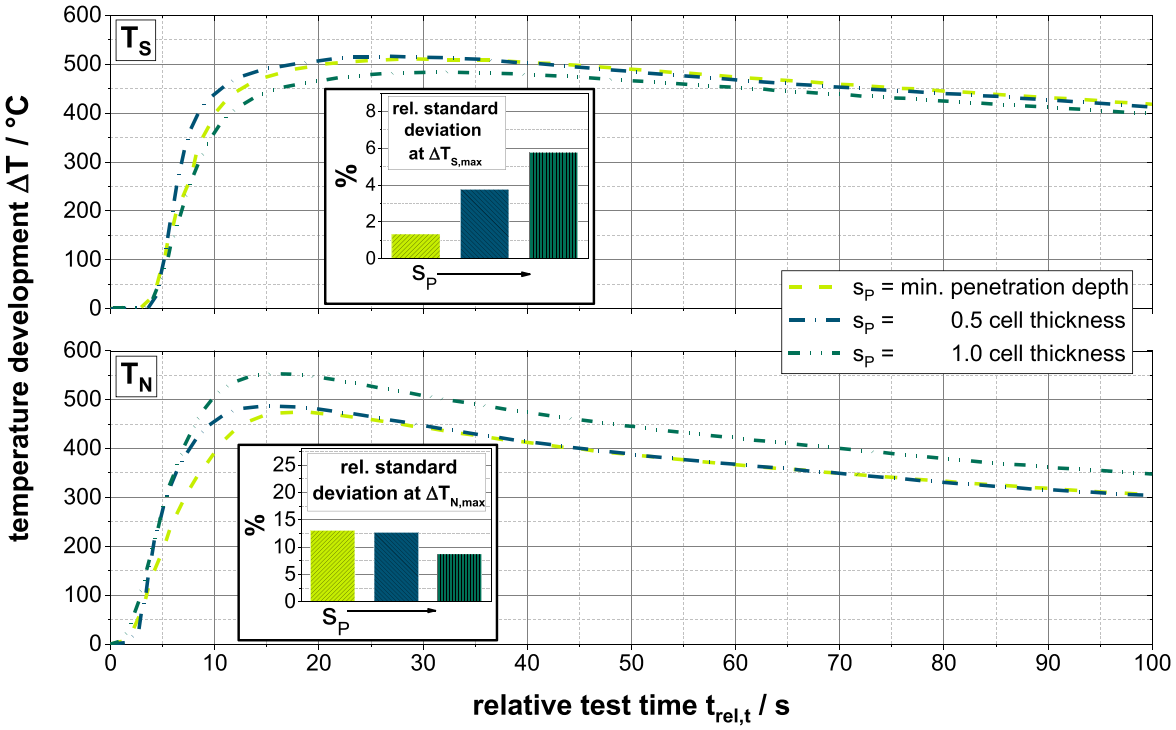

Figure 4. Average cell surface temperature ΔT_s and average developed nail temperature ΔT_N as function of the relative test time $t_{rel,t}$ for different nail penetration depths (nail speed $v_N = 80$ mm s^{-1}).

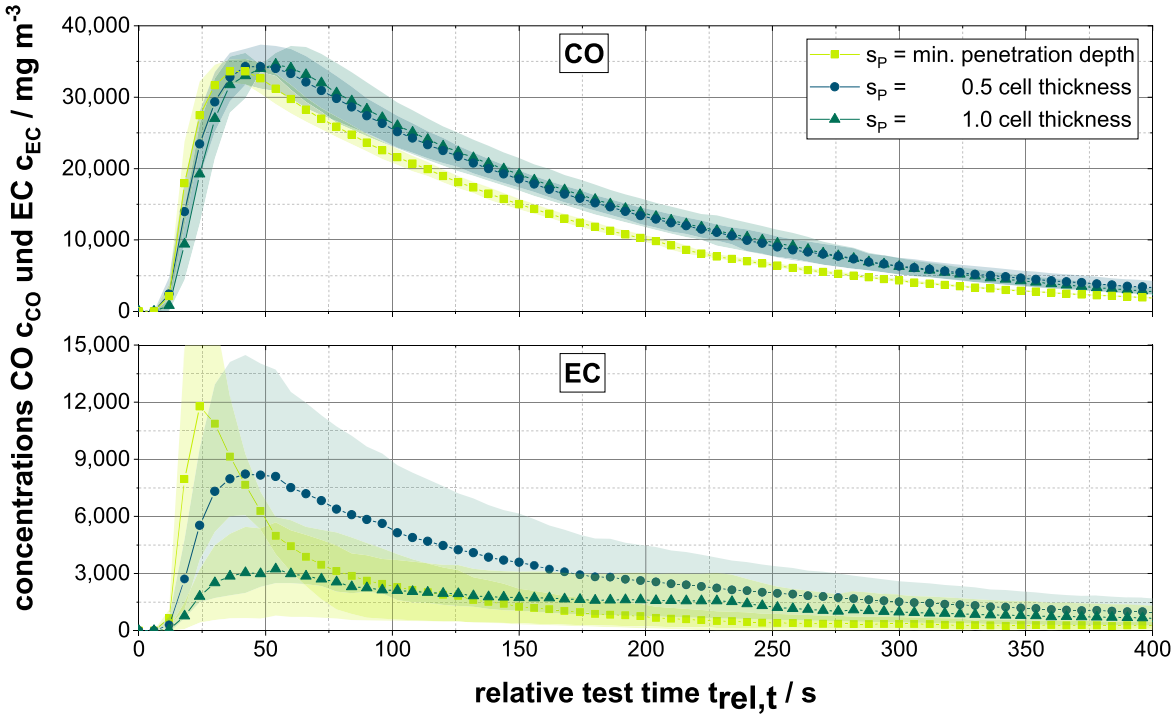

Figure 5. Concentrations of the gas components carbon monoxide (CO) c_{CO} and ethylene carbonate (EC) c_{EC} as a function of the relative test time $t_{rel,t}$ for the different nail penetration depths at a nail speed v_N of 80 mm s^{-1}.

for this is not the course of the TR or the number of short-circuited electrode layers, but the temporal release of the initial Joule heat. At greater penetration depths, in addition to the necessary activation energy which triggers a TR, further Joule heat is generated by a higher number of short-circuited electrode layers which can in turn influence the reactions taking place. Applying the minimum penetration depth only as many electrode layers as required for the reaction start are short-circuited within the accuracy of manual nail control. Thus, this test method leads to the lowest deviations for the relevant key parameters among the tests. Since only the initial voltage drop is decisive for the start of the TR, higher standard deviations of the cell voltage have little influence.

The automation of this test method through the development of the voltage-based nail control described in section 2 allows almost

identical triggering of a TR under specific test conditions with simultaneously high resolution of the covered nail path (0.01 mm). In addition, the relevant penetration depth $s_{rel,p}$, the covered nail distance between the first quick voltage change and the start of the TR can provide further information about parameter influences. The new test method was used for all tests presented in the following.

Nail speed and nail material.—In the following studies on the variation of the nail speed v_N for the conductive and the non-conductive nails are studied. This is to determine the limitations of the voltage-based nail control as well as to investigate the influence of the nail material on the short-circuit mechanism changes.

The triggers for a TR, the relevant penetration depth and the voltage drop for both nail variants, are shown for a variation of the nail speed in Fig. 6.

For the conductive nail, the cell voltages for all nail speeds exhibit a voltage drop to 0 V in a small time window, while the duration of the initial voltage drop differs between 1–10 mm s^{-1} and 40 and 80 mm s^{-1}.

The relevant penetration depth $s_{rel,p}$ increases up to a nail speed of 10 mm s^{-1}. This insignificant and very small increase with overlapping standard deviations has no significant influence on the voltage drop up to a relative test time $t_{rel,t}$ of 4.5 s. The initial voltage drop over 4.0 V is identical. The relevant penetration depth drops sharply at a nail speed of 40 mm s^{-1}. It is no longer measurable for 80 mm s^{-1} but the TR occurs immediately with the first detected change of cell voltage which results in a stronger initial voltage drop. While the cell voltage adjusts to the values of lower speeds when penetrating with a nail speed of 40 mm s^{-1}, the cell voltage decreases faster when penetrated with 80 mm s^{-1}.

The reason for this can be found in the penetration depth achieved at the first detected voltage change s_{P1} and the resulting absolute penetration depth s_P. s_{P1} rises with increasing speed because of the remaining time constants of the nail control and absolute penetration depths. Also, s_P are highest for the two fastest nail speeds.

The tests with a non-conductive nail generally show a slower initial voltage drop whereas the cell voltage of 0 V is reached later. The nail also penetrates much deeper into the cell before the TR is triggered. The smaller short-circuit cross section is responsible for this. While the entire cross-section is available for the current with a conductive nail, it is only the contact surface between the electrodes with a non-conductive nail. For this reason, the standard deviation of the relevant penetration depth $s_{rel,P}$ decreases with increasing speed and penetration depth. With a higher number of short-circuited electrode layers, deviations are less significant. The reason for the renewed increase in cell voltage at a nail speed of 40 mm s^{-1} is a low absolute penetration depth. To trigger the TR, only a few electrode layers are short-circuited, which leads to a renewed voltage increase with renewed contact of the intact electrodes after the melting of the separator and cell opening.

The differences in the courses of cell voltage can be found in the temperatures of the cell surface. Specifically it can be stated that the faster the initial voltage drop is (e.g. for 80 mm s^{-1}), the faster the increase and higher the maximum surface temperature ΔT_S (Fig. 7) occurs for both nail types. When using a conductive nail, the faster voltage drop is achieved by a higher penetration depth and thus a higher number of short-circuited electrode layers. This also creates a higher reaction surface inside the cell and the TR proceeds faster. Further evidence for the faster TR can be seen in the X-ray images of the cells before and after the tests with different nail speeds in Fig. 8.

The lighter areas of the cells posttests represent areas of lower solid densities and are therefore decisive for a higher mass loss. It becomes apparent that the lighter areas represent a mass transfer of gaseous reaction products as well as entrained solids from the penetration point to external. In all post-mortem images it can be seen that the contact area is a weak point. The transport routes to the outside widen with increasing nail speed. Especially at a nail speed v_N of 80 mm s^{-1} it becomes clear that considerably more mass transport pathways are created. Since the total mass losses of the cells after the tests show no dependence on the nail speed, this effect can be explained by the speed of the mass loss as well as the speed of the TR.

A faster TR can also be seen in the concentrations of the gaseous component CO in Fig. 9. While the concentrations for nail speeds v_N 1–10 mm s^{-1} are similar when using a conductive nail, the

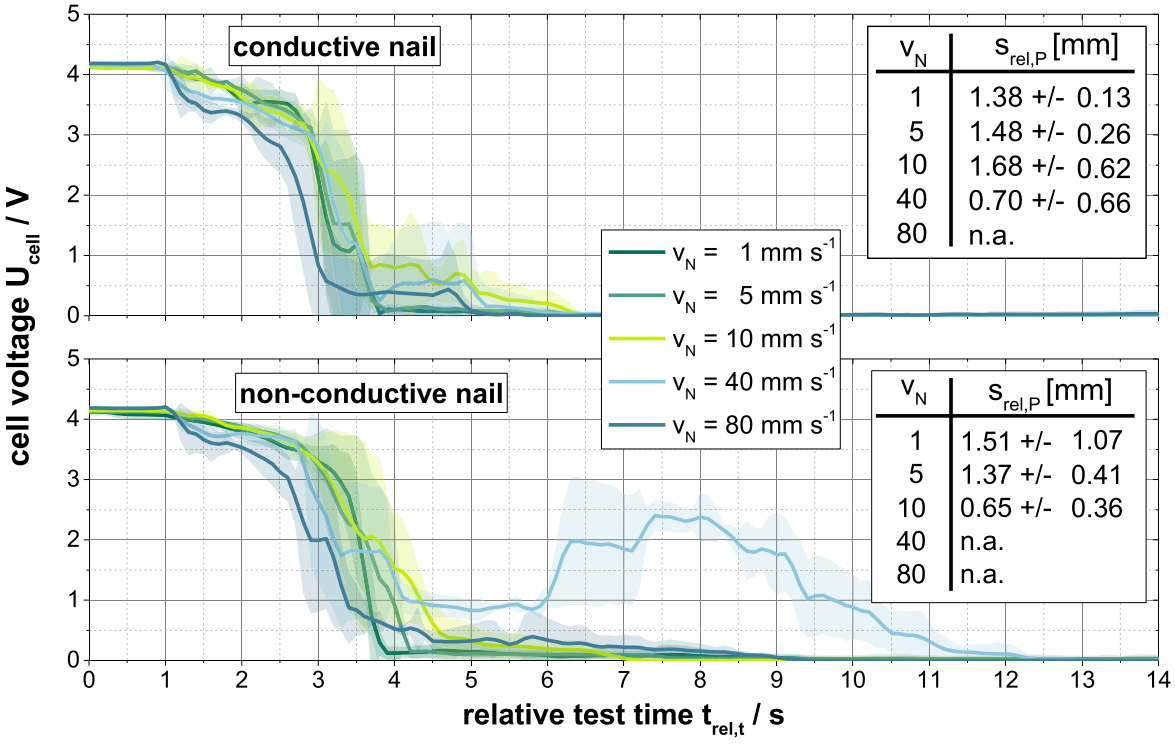

Figure 6. Average cell voltage U_{cell} as a function of the relative test time $t_{rel,t}$ for different nail speeds v_N and with a conductive and non-conductive nail (standard deviation by triple determination).

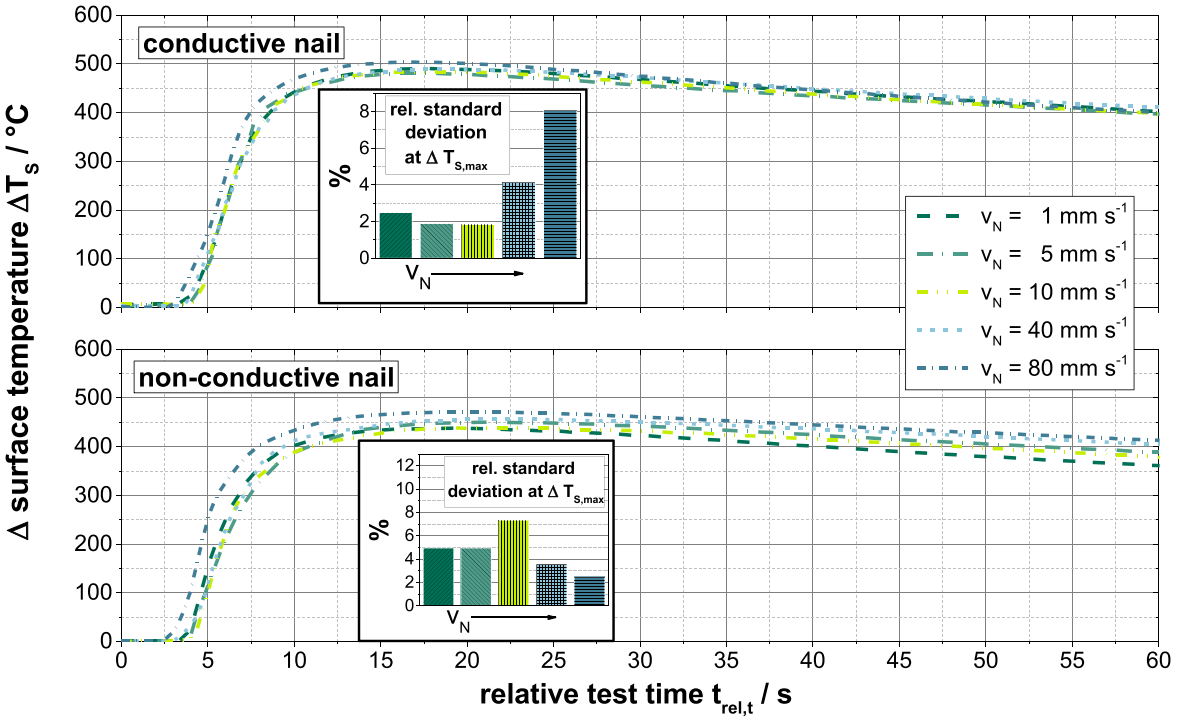

Figure 7. Average cell surface temperature ΔT_S as a function of the relative test time $t_{rel,t}$ for different nail speeds v_N and with a conductive and non-conductive nail, as well as the standard deviation of a triple determination at the maximum cell surface temperature $\Delta T_{S,max}$.

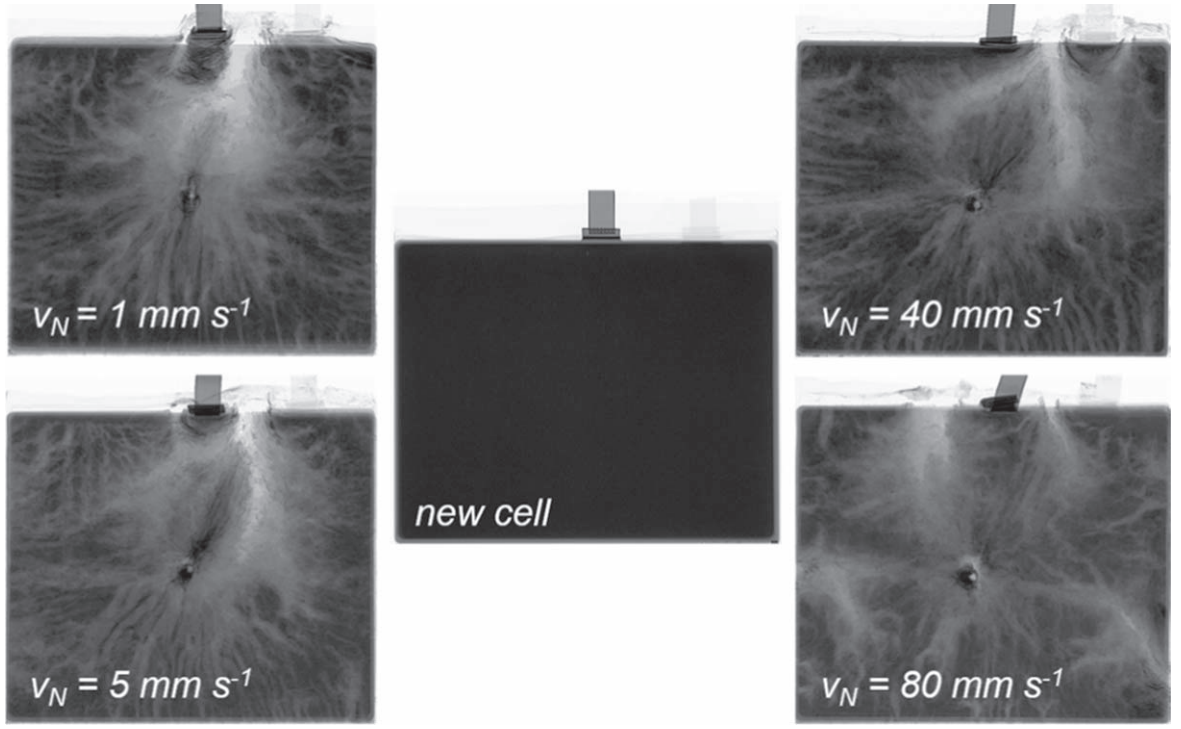

Figure 8. X-ray images of a new cell and already tested with different nail velocities v_N 1–80 mm s^{-1} cells.

concentrations for v_N 40 and 80 mm s^{-1} increase significantly faster. At the highest nail speed the highest maximum concentrations are achieved. A high penetration depth reached at high speed leads to fast initial reactions. Since CO is mainly formed by the initial reactions between intercalated Li and the carbonates of the electrolyte[18–20] they are preferred. Furthermore, the educts and the solvents of the electrolyte, are available as they have not yet evaporated. This leads to a fast increase of the surface temperature as well as CO concentrations.

The results for the released concentrations of HF reflect a faster course of the TR for higher nail speeds (40 and 80 mm s^{-1}), whereas HF concentrations for the nail speeds of 1, 5 and 10 mm s^{-1} are in the same order of magnitude. Higher concentrations are achieved at a nail speed of 80 mm s^{-1}. In addition to a higher TR speed, the

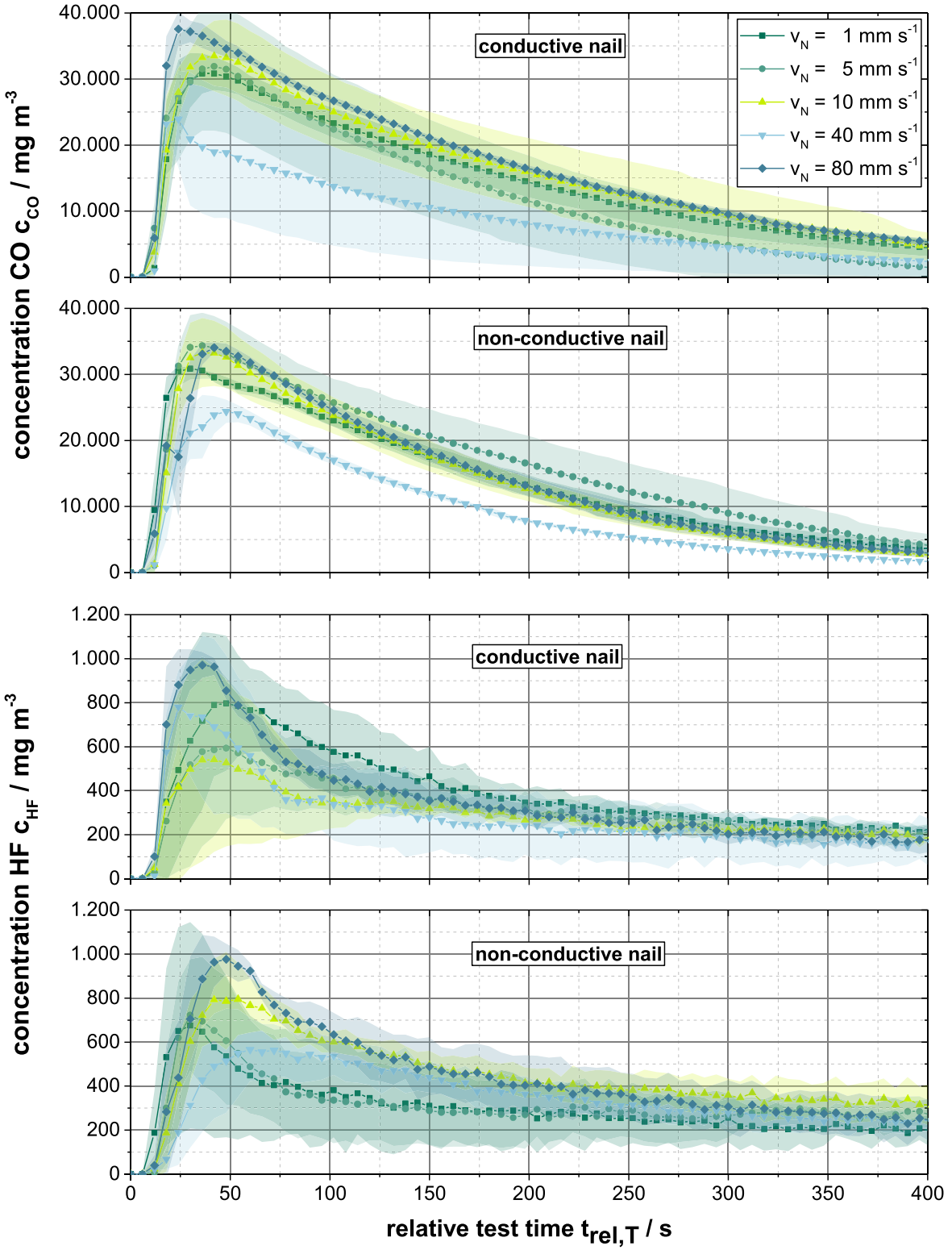

Figure 9. Concentrations of the gas component carbon monoxide (CO) c_{CO} and of hydrogen fluoride (HF) c_{HF} depending on the relative test time $t_{rel,t}$ at different nail speeds and for a conductive and a non-conductive nail, as well as the standard deviation of a triple determination.

higher cell surface temperature is of influence in this context, since the endothermic decomposition of the PVDF binder is an additional source of HF.

For the variation of the nail speed with a non-conductive nail no significant trend can be detected for either of the gas components.

In regards to the method development, special attention needs to be paid to the standard deviations again. The relative standard deviations of the surface temperature up to its maximum are of particular interest. If a conductive nail is used, the deviations are at a similarly low level up to a nail speed of 10 mm s^{-1} and then rise significantly for faster speeds.

When using a non-conductive nail, the relative standard deviations are generally higher. This can be explained by the randomness of the actual short circuits. While all contacted electrode layers are

short-circuited with a conductive nail, this is not necessarily the case with a non-conductive nail as only the electrodes themselves are short-circuited. If a short circuit in one compartment occurs, the adjacent electrode layers are not necessarily affected. A direct association of standard deviations can be established for the relevant depth of penetration and concentrations of CO. A large expressed deviation of the relevant penetration depth in turn results in a high deviation of the gas concentration and vice versa.

In summary, the use of a conductive nail achieves more reproducible and meaningful data regarding penetration depth, temperature and gas concentrations. It becomes clear that the applied method of voltage-based nail control reaches its limits for nail speeds of $\geqslant 40\,\mathrm{mm\,s^{-1}}$, which is caused by the time-dependent switching. The triggering of the control is always set to the same time constants and thus, reacts relatively slower at higher nail speeds. The small standard deviations for the cell voltage, the relevant penetration depth and the surface temperatures lead to the determination of $1\,\mathrm{mm\,s^{-1}}$ nail speed as a standard for a reliable and reproducible test setup. The here presented results suggest that nail speed and penetration depth have an influence on the speed of the TR.

Conclusions

The results presented in this work lead to a new method for performing nail penetration tests of high reproducibility. The new method involves clamping the cells to be tested using a glass fibre tape to minimize heat dissipation and enable a more realistic temperature measurement. A nitrogen atmosphere is recommended to measure the resulting gas components of interest with high reproducibility.

The voltage-based nail control is an essential key element of the measurement device and the new method, as it makes it possible to generate a defined short circuit. Firstly, this short circuit is always the same for one parameter setup and thus, overall enables a small standard deviation. Secondly, this type of nail control allows to realize a high resolution of the nail's penetration depth. Subsequently a statement can be made about the energy required to trigger a thermal runaway by means of the relevant nail penetration depth and the number of short-circuited electrode layers.

In particular, a low nail speed of $1\,\mathrm{mm\,s^{-1}}$ is suitable to achieve low standard deviations. Because of low standard deviation a conductive nail should be used. Reason for this is the fundamentally different way of triggering short circuits. While the non-conductive nail only produces undefined short-circuits through direct electrode contact, the conductive nail can contact the electrodes through itself, resulting in lower deviations and more reproducible short-circuits.

The use of this method makes it possible, specifically due to low standard deviations, to determine correlations between nail penetration depth and, correlating voltage drop as well as resulting cell surface temperatures and concentrations of the gas components. However, this has to be discussed in more detail by further parameter studies and cell variations. Furthermore, the number of cells that need to be used for destructive testing can be reduced to three cells resulting in time and cost savings in the cell development process.

Acknowledgments

The authors thank the German Federal Ministry for the Environment, Nature Conservation, Building and Nuclear Safety for the funding of research project LithoRec II (Reference No. 16EM1024). This project enabled the basic conception and realization of the test stand, even though the development of the method presented took place after project completion. Furthermore, thank you to Marcel Wuwer and Markus Moeller from Viscom AG for the preparation of X-ray images of the cells. The authors also thank Uwe Stüwe, Ernst Jelting, Alexander Diener, Joachim Schneider, and Detlev Hille for the technical support in the realization of the test stand and the method.

ORCID

Jan Diekmann https://orcid.org/0000-0001-7527-7563

References

1. V. Etacheri, R. Marom, R. Elazari, G. Salitra, and D. Aurbach, *Energy Environ. Sci.*, **4**, 3243 (2011).
2. B. Scrosati and J. Garche, *J. Power Sources*, **195**, 2419 (2010).
3. N. Nitta, F. Wu, J. T. Lee, and G. Yushin, *Mater. Today*, **18**, 252 (2015).
4. Q. Wang, P. Ping, X. Zhao, G. Chu, J. Sun, and C. Chen, *J. Power Sources*, **208**, 210 (2012).
5. P. G. Balakrishnan, R. Ramesh, and T. Prem Kumar, *J. Power Sources*, **155**, 401 (2006).
6. S.-I. Tobishima, K. Takei, Y. Sakurai, and J.-I. Yamaki, *J. Power Sources*, **90**, 188 (2000).
7. V. Ruiz, A. Pfrang, A. Kriston, N. Omar, P. van den Bossche, and L. Boon-Brett, *Renew. Sustain. Energy Rev.*, **81**, 1427 (2018).
8. L. Greve and C. Fehrenbach, *J. Power Sources*, **214**, 377 (2012).
9. B. Liu, S. Yin, and J. Xu, *Appl. Energy*, **183**, 278 (2016).
10. H. Yang, H. Bang, K. Amine, and J. Prakash, *J. Electrochem. Soc.*, **152**, A73 (2005).
11. H. Yang, G. V. Zhuang, and P. N. Ross, *J. Power Sources*, **161**, 573 (2006).
12. N. E. Galushkin, N. N. Yazvinskaya, and D. N. Galushkin, *J. Electrochem. Soc.*, **165**, A1303 (2018).
13. H. Wang, A. Tang, and K. Huang, *Chin. J. Chem.*, **29**, 1583 (2011).
14. C. F. Lopez, J. A. Jeevarajan, and P. P. Mukherjee, *J. Electrochem. Soc.*, **162**, A1905 (2015).
15. N. S. Spinner, C. R. Field, M. H. Hammond, B. A. Williams, K. M. Myers, A. L. Lubrano, S. L. Rose-Pehrsson, and S. G. Tuttle, *J. Power Sources*, **279**, 713 (2015).
16. M. Zhang, J. Du, L. Liu, A. Stefanopoulou, J. Siegel, L. Lu, X. He, X. Xie, and M. Ouyang, *J. Electrochem. Soc.*, **164**, A3038 (2017).
17. T. D. Hatchard, S. Trussler, and J. R. Dahn, *J. Power Sources*, **247**, 821 (2014).
18. G. Gachot, P. Ribière, D. Mathiron, S. Grugeon, M. Armand, J.-B. Leriche, S. Pilard, and S. Laruelle, *Anal. Chem.*, **8**, 8 (2011).
19. M. Onuki, S. Kinoshita, Y. Sakata, M. Yanagidate, Y. Otake, M. Ue, and M. Deguchi, *J. Electrochem. Soc.*, **155**, A794 (2008).
20. D. Aurbach, I. Weissman, A. Schechter, and H. Cohen, *Langmuir*, **12**, 3991 (1996).